# Phase Combining Strategies for Polarization-Independent Demodulation in a DAS Using Homodyne Detection with Delayed Self-Mixing in a Non-Stabilized Mach-Zehnder Interferometer

Almaz Demise, Fabrizio Di Pasquale and Yonas Muanenda

*Institute of Mechanical Intelligence, Scuola Superiore Sant'Anna, Via Giuseppe Moruzzi, 1, Pisa, Italy*

Abstract:     We investigate a suitable polarization diversity algorithm for mitigating polarization fading in phase demodulation in a φ-OTDR based on a delayed Mach-Zehnder interferometer (MZI) and a polarization-diversity 90-degree optical hybrid. The intermediate components of the signal are combined using four different strategies employing weighing factors calculated from the SNR of the in-phase component and visibility of backscattering amplitude in the slow and fast axes to suppress polarization fading in distributed dynamic phase measurements. We compare the algorithms in terms of suitability for suppressing fading and added computational times. The proposed technique uses a single compact amplifier at the source and employs delayed self-mixing in an unbalanced MZI, thereby relaxing the requirement of temperature and phase isolation in the receiver interferometer. Experimental results show that, while all combining strategies mitigate fading, the selection of higher SNR of the in-phase component at the far end yields the best results in terms of ease of computation and could accurately detect weak acoustic signals at the end of a 10-km sensing fiber with a frequency of 2 kHz in the presence of fading in a single polarization.

## 1 INTRODUCTION

Distributed acoustic sensing (DAS) is a widely used dynamic monitoring technique that enables simultaneous, real-time detection of vibrations caused by events over a long span of an optical fiber and has attracted much attention in recent years (Rao et al., 2021 & Demise et al., 2023). A DAS system is based on probing an optical fiber with a coherent laser fiber and recording the coherent Rayleigh backscattering along the fiber, which is sensitive to phase changes caused by vibrations or changes in temperature. A common implementation is a phase-sensitive optical time domain reflectometer (φ-OTDR), which involves sending a narrow linewidth laser along the fiber and mapping the evolution of the coherent Rayleigh backscattering signal intensity and phase along each position (Zhang et al., 2016 & Muanenda, 2018). Recently DAS interrogation schemes based on Mach-Zehnder interferometers and modulators suitable for photonic integration on a silicon photonics platform (Jin et al., 2024) which has been proven to be attractive for its use in many applications including those in harsh environments (Cammarata et al., 2022). In the past, research on DAS has been focused on the design of a compact source for programmable complex chirp waveforms for enhancing the spatial resolution (Demise et al., 2024) as well as the use of data storage and cloud computing for real-time applications (Nur & Muanenda, 2024).

In a conventional φ-OTDR, responses induced by acoustic signals are obtained by simply demodulating the amplitude of Rayleigh backscattering (RBS) light waves (Uyar et al., 2019). However, the amplitude signal varies nonlinearly with the strain of the sensing fiber, which can distort the acquired acoustic signal. Coherent detection has been proven to be an effective approach to boost the performance of intensity demodulation and is also naturally adapted to phase demodulation in φ-OTDR (Shaheen et al., 2023 & Li et al., 2022). However, coherent detection is susceptible to polarization mismatch between the measured and reference signals; hence, polarization-induced fading can greatly affect measurement accuracy (Stowe et al., 1982). The polarization mismatch would decrease the SNR of φ-OTDR time-domain traces and cause the low visibility of interference signals.

Wang (Wang et al., 2016) proposed a phase extraction method for single polarization that employs coherent homodyne detection using a 90° hybrid and a local oscillator (LO), in which the backscattering signal is fed to the input of the 90° hybrid along with a local oscillator to obtain the two orthogonal components. This experiment shows the ability of a 90-degree hybrid to measure in-phase and quadrature components simultaneously, in the case of the incoming signal polarization is aligned with that of a LO. However, in a real system, the birefringence of the transmission fiber changes randomly, and the polarization of the incoming signal is unlikely to remain aligned with the state of polarization (SOP) of the LO. To address this problem, not only should polarization diversity be introduced into the coherent receiver, but also it should be implemented in the best possible way to suppress fading.

In this work, we experimentally demonstrate a homodyne phase-demodulation technique in a DAS based on delayed self-mixing with polarization diversity hybrid and I/Q demodulation. Unlike schemes in which the laser is used as a local oscillator, our scheme does not necessitate the coherence of the probing source to be as long as the sensing distance. Both the x and y polarizations of the I and Q components of the beat signal are obtained directly without averaging, and different polarization fading suppression algorithms are employed to obtain the demodulated phase along a 10-km fiber induced by small vibrations. Experimental results show that not only it is important to pay attention to how the final phase is calculated but also is it critical to choose a suitable combining strategy to obtain the phase from the I/Q components in the fast and slow axes of polarization. The proposed system could successfully acquire the acoustic signal information induced by weak vibrations at the end of the sensing fiber, including the location, frequency, amplitude, and phase simultaneously.

## 2 THEORY

Coherent optical systems permit low signal-to-noise ratio and compensate for several types of propagation impairments while preserving phase information of the optical signal. When a pulse of light from a highly coherent laser source is sent along the sensing fiber, the phase change of the backscattered coherent Rayleigh light contains the vibration information (Liu et al., 2022 & Yang et al., 2016).

Coherent systems operating with a single polarization typically include a coherent receiver that

mixes the received signal with LO, thereby operating at a frequency close to the received signal and hence requiring heterodyne detection with higher detection bandwidth. The balanced detection suppresses the common-mode noise and maximizes the beat between the signal and the LO. However, due to the transmission fiber's randomly varying birefringence, backscattering signal polarization is not always aligned with the LO polarization. To solve the resulting problem of fading, polarization diversity receivers were introduced in coherent receivers.

Figure 1 shows the configuration of a generic polarization diversity coherent receiver, wherein two single-polarization receivers are combined. First, the incoming RBS signal with an arbitrary SOP is separated into two linear polarization components, these having the same frequency as the LO light with a polarization beam splitter (PBS); $I_x$, $Q_x$, $I_y$, and $Q_y$ are the photocurrent outputs of the four balanced detectors. Balanced photodetector (BPD) output retains only alternating current signals while removing direct current signals.
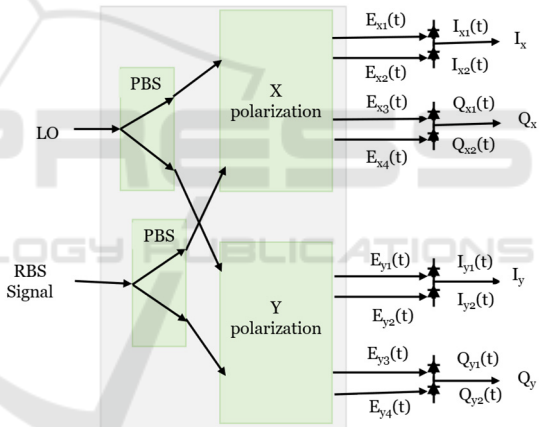


Figure 1: Generic configuration of polarization diversity hybrid with balanced photodiodes (90° Optical Hybrid Manual).

The complex electric field of the RBS signal in φ-OTDR is expressed as:

$$E_s(t) = A_s(t)\exp\{j(\omega_s t + \theta_s(t) + \theta(t))\} \qquad (1)$$

where $A_s(t)$, $\omega_s$, and $\theta_s(t)$ are the complex amplitude, angular frequency, and the initial phase of the signal, respectively. The term $\theta(t)$ stands for the phase change induced by perturbations along the fiber.

Similarly, the complex electric field of the LO used as a reference at the receiver can be written as:

$$E_l(t) = A_l(t)\exp\{j(\omega_l t + \theta_l(t))\} \qquad (2)$$

where $A_l(t)$, $\omega_l$, and $\theta_l(t)$ are the complex amplitude, the angular frequency, and the phase of the local oscillator, respectively.

The incoming signal having an arbitrary SOP is separated into two linearly polarized components (along the x and y axes with a PBS, which are equally split into two arms by the 90-degree optical hybrid, and the corresponding light field becomes:

$$E_{sx,y}(t) = \frac{1}{2} A_{sx,y}(t) \exp j\{(\omega_s t + \theta_s(t) + \theta(t))\} \tag{3}$$

where $E_{sx,y}(t)$ and $A_{sx,y}(t)$ are the complex electric field and amplitude of the transmitted signal of both polarizations respectively. $E_{sx,y}(t)$ represents the complex electric field of the signal in the x and y polarization ($E_{sx}(t)$ and $E_{sy}(t)$) and the coefficient ½ comes from the equal splitting of the signal.

The LO signal is also split into two arms, one of which is phase-shifted by 90° resulting in (Wang et al., 2016):

$$\frac{1}{2} A_{lx,y}(t) \exp \left\{ j \left( \omega_l t + \theta_l(t) + \frac{\pi}{2} \right) \right\} = \frac{1}{2} j E_{lx,y}(t) \tag{4}$$

where $E_{lx,y}(t)$ and $A_{lx,y}(t)$ are the complex electric field and amplitude of LO in both polarizations respectively.

Each branch of the LO signal is coupled with the respective branch of the RBS signal giving rise to the eight outputs of the PDH:

$$E_{x,y1}(t) = \frac{1}{2\sqrt{2}} (E_{sx,y}(t) + E_{lx,y}(t))$$
$$E_{x,y2}(t) = \frac{1}{2\sqrt{2}} (E_{sx,y}(t) - E_{lx,y}(t))$$
$$E_{x,y3}(t) = \frac{1}{2\sqrt{2}} (E_{sx,y}(t) + jE_{lx,y}(t))$$
$$E_{x,y4}(t) = \frac{1}{2\sqrt{2}} (E_{sx,y}(t) - jE_{lx,y}(t)) \tag{5}$$

The beating at BPDs (Bielecki et al., 2022) can then be written as:

$$I_{x,y1}(t) = \frac{R}{8} [(A_{sx,y}(t))^2 + (A_{lx,y}(t))^2 + 2A_{sx,y}(t)A_{lx,y}(t) \cos\{(\omega_s - \omega_l)t + (\theta_s(t) - \theta_l(t)) + \theta(t)\}]$$

$$I_{x,y2}(t) = \frac{R}{8} [(A_{sx,y}(t))^2 + (A_{lx,y}(t))^2 - 2A_{sx,y}(t)A_{lx,y}(t) \cos\{(\omega_s - \omega_l)t + (\theta_s(t) - \theta_l(t)) + \theta(t)\}] \tag{6}$$

where R is the responsivity of all detectors, which is assumed to be the same.

The balanced photodetectors can detect small differences in optical power between two optical input signals while largely suppressing any common fluctuations of the inputs. With the help of BPD, the DC signals can be filtered out and the resulting RF signal can be expressed as:

$$I_{x,y}(t) = I_{x,y1}(t) - I_{x,y2}(t) = \frac{R}{4} A_{sx,y}(t) A_{lx,y}(t) \cos\{(\omega_s - \omega_l)t + (\theta_s(t) - \theta_l(t)) + \theta(t)\} \tag{7}$$

Similarly, applying equations (6) and (7) for the quadrature component we obtain:

$$Q_{x,y}(t) = \frac{R}{4} A_{sx,y}(t) A_{lx,y}(t) \sin\{(\omega_s - \omega_l)t + (\theta_s(t) - \theta_l(t)) + \theta(t)\} \tag{8}$$

In our experiment, the input to the LO part of the hybrid is the time-delayed replica of the one at the signal input, namely:

$$E_l(t) = A_{delayed}(t) \exp \{ j (\omega_s.(t - \tau) + \theta_s + \theta(t - \tau)) \} \tag{9}$$

Appling equation (9) for equations (7) and (8):

$$I_{x,y}(t) = \frac{R}{4} A_{sx,y}(t) A_{delayedx,y}(t) \cos\{\varphi(t) + \varphi_c\} \tag{10}$$

$$Q_{x,y}(t) = \frac{R}{4} A_{sx,y}(t) A_{delayedx,y}(t) \sin\{\varphi(t) + \varphi_c\}$$

where $\varphi(t)$ is the detected phase change due to external vibration and $\varphi_c$ is the constant phase change due to the delaying interferometer and it can be removed when subtracting phases of two certain positions.

Subsequently, the distributed phase is calculated from the I/Q components of each polarization axis so that:

$$\varphi_i = \tan^{-1}\left(\frac{Q_i}{I_i}\right) \tag{11}$$

Implementing the phase unwrapping algorithm on the output of the arctan function extends the demodulated phase range from negative infinity to positive infinity. The differential phase with respect to an adjacent point in the fiber was used to measure the phase change induced by vibrations.

$$\Delta\varphi = \varphi_{z1}(t) - \varphi_{z2}(t) \qquad (12)$$

Conventional polarization-diversity phase measurement schemes assume that the contributions of the fast and slow axes of polarization to the phase extraction are the same, and the phase is obtained by combining the contributions from the two with equal weight. However, the signals in both axes could differ in terms of SNR values in both the in-phase and quadrature as well as the visibility of the amplitude of the backscattering traces. Hence new strategies that take into account these parameters for each measurement round could be devised. In this contribution, we employ the tracking of the relative SNR of the in-phase component of each polarization axis and the mean interference visibility of the amplitude at the far end of the fiber which is used for determining a suitable contribution strategy. Specifically, we use percentage ratios of the relative SNR and visibility terms to weigh the contribution of each axis to the calculated phase or select the phase of the one that has a better SNR in its in-phase component. We compare the results with the conventional approach and conclude that these algorithms help to detect very low-intensity vibrations at the far end of the fiber with minimal post-processing in the presence of fading, with selection of the phase contribution from the axis with higher SNR yielding a relatively better result.

## 3 EXPERIMENTAL SETUP

The experimental setup of the φ-OTDR based on the polarization diversity hybrid scheme is shown in Figure 2.

The continuous-wave light emitted by a narrow linewidth laser source operating at 1550 nm and with a linewidth of 100 Hz was amplified by an erbium-ytterbium doped fiber amplifier (EYDFA) and injected into an acoustic-optic modulator (AOM) to generate a pulsed light. An arbitrary waveform generator (AWG) is then used to generate pulses having a width of 100 ns and a repetition rate of 8.33 kHz. A 1.2 nm linewidth optical bandpass filter (OPBF) with an operating wavelength from 1530 nm to 1560 nm suppresses the EYDFA's amplified spontaneous emission (ASE) noise. The amplified pulses are then launched through a three-port circulator into the fiber under test (FUT), which is a 10 km standard single-mode fiber, a short segment of the far end is wounded around a cylinder piezoelectric transducer (PZT) driven with a voltage amplifier connected to a waveform generator for applying waveforms of controlled frequency. To investigate the ability of the proposed system to detect phase changes in the presence of polarization fading, the PZT was driven with voltage values close to the minimum possible peak-to-peak input.

The RBS light was amplified and filtered by another EDFA and bandpass filter to improve the SNR of the signal in the presence of the optical hybrid (which typically has an insertion loss of 7-8 dB); it was then fed through a delayed self-mixing interferometer using a 3 dB coupler. One arm of the interferometer is connected to the signal port of the polarization diversity hybrid (PDH) and the other is delayed by a 20 m single-mode fiber and fed to the LO of the PDH. A polarization controller (PC) is placed at the LO input of the optical hybrid to adjust the angle polarization in the same branch. The fiber length used for the delay is carefully chosen so that the back reflections of two adjacent pulses overlap accurately.

The PDH consists of two single-polarization 90° optical hybrids that enable the extraction of phase, and amplitude, from a signal with any polarization. Eight outputs of the PDH were given to the four BPDs with a 100-MHz bandwidth. The sync output channel of AWG is used for triggering the signal and the beat electric signals from each BPD were sampled by a four-channel DAQ at a sampling rate of 156 MS/s, for subsequent processing.
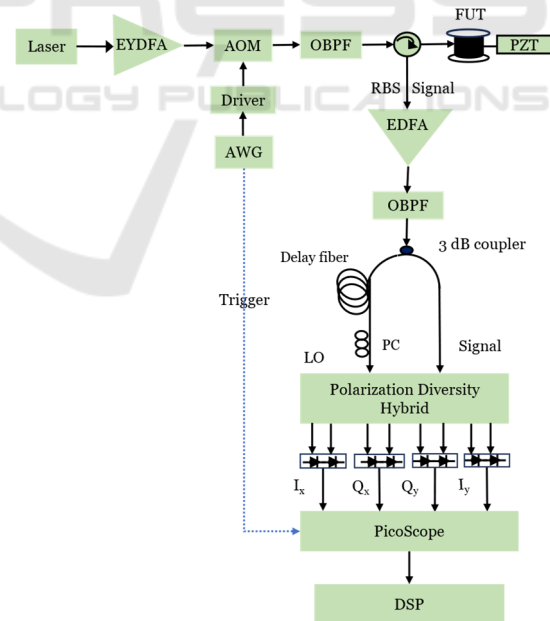


Figure 2: Scheme of delayed self-mixing with polarization diversity hybrid. EYDFA: Erbium-Ytterbium Fiber-Doped Amplifier; EDFA: Erbium-doped Fiber Amplifier; OBPF: Optical Band-Pass Filter; AOM: Acousto-Optic Modulator; AWG: Arbitrary Waveform Generator; DSP: Digital Signal Processing; FUT: Fiber Under Test; PZT: Piezoelectric Transducer; PC: Polarization Controller.

# 4 EXPERIMENTAL RESULTS AND DISCUSSIONS

Figure 3 shows the amplified Rayleigh backscattering traces before they are delayed and fed to the polarization diversity hybrid, indicating that the scheme has a high SNR of the backscattering signal.
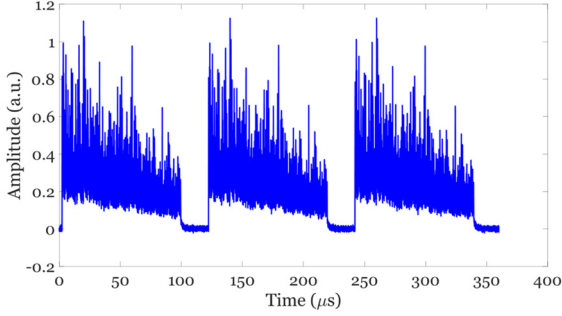


Figure 3: Row backscattering traces before the hybrid.

Using a 3 dB coupler, the amplified RBS was fed through a delayed self-mixing interferometer as a signal and LO. Figure 4 shows the overlaps of the raw $I_x$, $Q_x$, $I_y$, and $Q_y$ after the PDH, proving the RBS traces have high SNR and exhibit common-mode noise suppression.
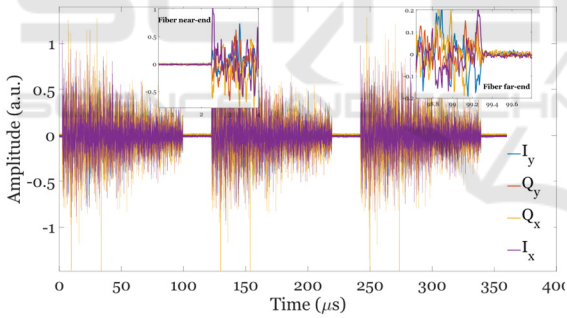


Figure 4: Overlapped raw traces for all 4 polarization components.

Subsequently, a sinusoidal signal of 2 kHz was applied to the PZT at the end of the fiber with a low driving voltage of 40 mV peak-to-peak. After minimal post-processing involving no averaging, the amplitude and phase of the x and y polarization components are reported in Figure 5 (a) and (b). The SNRs of the two polarized signals vary with the polarization of backscattering lights into the two input arms of the PDH, x and y polarizations have slightly different peak-to-peak power for both amplitude and phase traces.
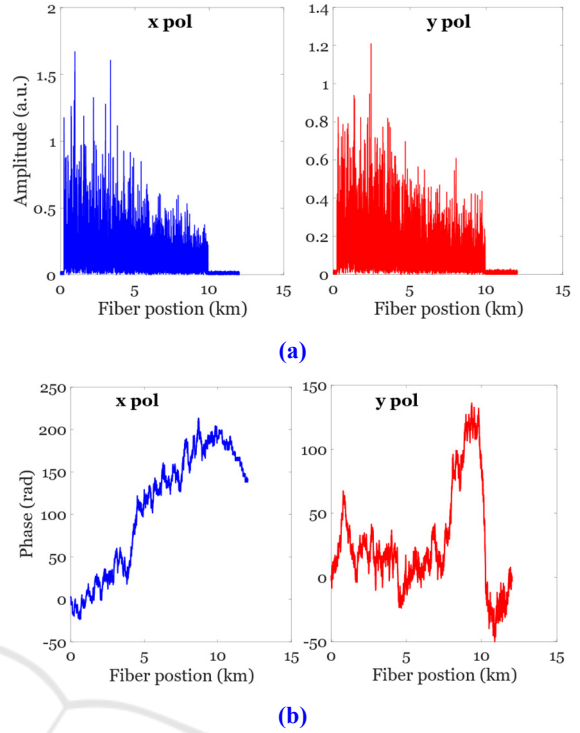


(a)



(b)

Figure 5: Demodulated responses for x and y polarization. (a) amplitude traces (b) unwrapped phase traces.

Then, we calculated the distributed phase for each of the fast and slow polarization axes and, for combining to suppress fading, employed four fading-suppression algorithms on the acquired 416 coherent backscattering traces along the fiber. The equal sum algorithm assumes that the contributions to the phase of the I/Q components in the x and y polarization have equal weights. In this case, the combined phase will have equal contributions from both polarizations. Figure 6 shows the unwrapped phase power spectra for x and y polarization and the one obtained with an equal sum algorithm.
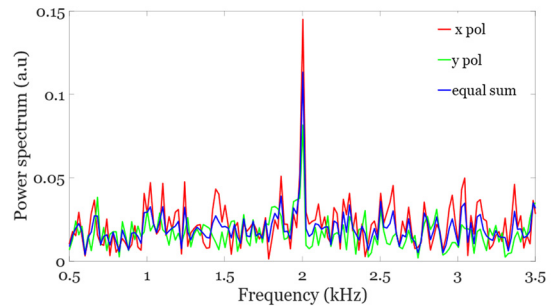


Figure 6: Comparison of unwrapped phase power spectra of equal sum with x and y polarization.

Selective higher SNR algorithm computes the phase response from the polarization axis with higher SNR. Figure 7 compares the selective SNR algorithm with individual polarizations. It shows that the demodulated phase for x polarization has a higher SNR, and the selective SNR algorithm uses the phase calculated from this component.
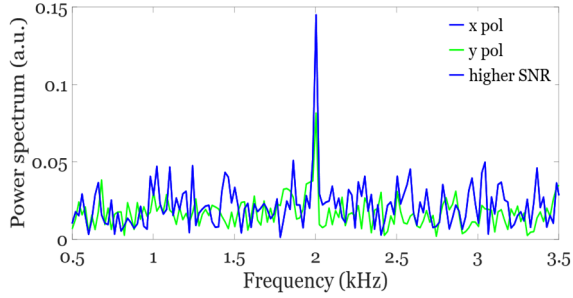


Figure 7: Selective higher SNR algorithm with x and y polarizations.

In the weighted-SNR algorithm, first, the SNR values of the in-phase components in the x and y polarization were calculated as the ratio of the RMS value of the speckle pattern at the end of the fiber and that of the noise floor, which represents the worst-case scenario for the entire sensing range. Then a multiplicative factor α is calculated as follows:

$$\alpha = \frac{SNR_1}{SNR_1 + SNR_2} \tag{13}$$

where $SNR_1$ and $SNR_2$ are the SNR of the in-phase components of both polarizations. Then the individual values are obtained as a weighted sum of α and (1-α) as:

$$SNR_{output} = \alpha * \Delta\varphi_1 + (1 - \alpha) * \Delta\varphi_2 \tag{14}$$

where $\Delta\varphi_1$ and $\Delta\varphi_2$ are the phase changes obtained from the I/Q components of the x- and y-polarization axes. Figure 8 shows the comparison of phase-weighted SNR with x and y polarizations.
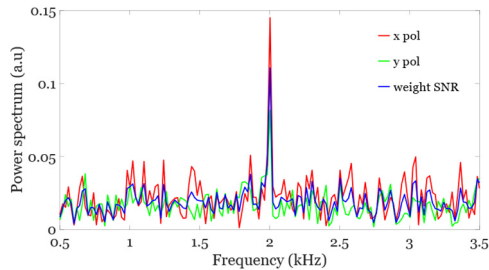


Figure 8: Phase obtained using weighted-SNR algorithm with x and y polarization.

Given the visibility in the amplitude traces is always higher than the visibility of the phase, we can calculate the multiplicative factor from the amplitude traces. The last algorithm called weighted-visibility is based on the computation of alpha visibility ($\alpha_v$) which is the ratio of the net visibility for a segment of fiber at the far end as shown in Figure 9 and is calculated as:
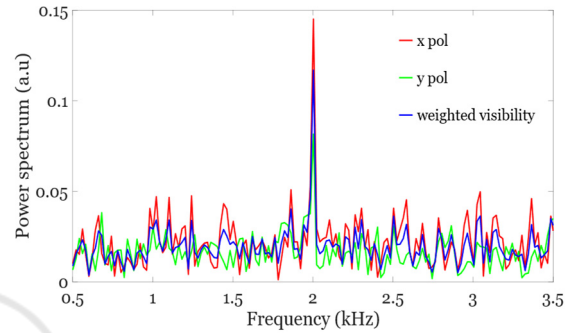
$$\alpha_v = \frac{\chi_1}{\chi_1 + \chi_2} \tag{15}$$



Figure 9: Phase-weighted visibility SNR algorithm with x and y polarizations.

The weighed visibility $\chi i$ for each polarization of the backscattering signal for a short span at the end of the fiber was calculated by first dividing the end of the fiber into discrete bins and computing the mean of the interference visibility $\chi n$ calculated for each bin as:

$$\chi_n = \frac{Ai_{max} - Ai_{min}}{Ai_{max} + Ai_{min}} \tag{16}$$

where $Ai_{max}$ and $Ai_{min}$ are the minimum and maximum values of the amplitudes of the backscattering signals within each bin. Thus, as opposed to just having a single visibility value, is done to have the best possible representation of visibility, thereby avoiding the possibility of one extreme case of execution of the speckle pattern resulting in a wrong evaluation of the relative visibility for both polarizations.

A comparison of the performance of the four combining algorithms for polarization-diversity phase demodulation in the $\varphi$-OTDR system is depicted in Figure 10. It is seen that all algorithms help suppress the effect of fading, the higher SNR selective algorithm yields a comparatively better location and phase change detection in the vicinity of the applied disturbance. In addition to confirming the computation and monitoring of the SNR and visibility of the amplitude of the backscattering at the end of the fiber being critical to fading-suppressed phase change detection, our

analysis points to the choice of the strategy of choosing the polarization axes yielding higher SNR in the in-phase component as being promising as it also entails lowest computational cost among the algorithms considered.

Comparing the performance of four combining algorithms for polarization-independent measurements in the $\varphi$-OTDR system, the performance of the selective higher in-phase SNR algorithm is optimal. Note that the selection of the phase contribution is made solely based on which axis has a high SNR in its in-phase component in a single measurement round of 416 traces spanning an interval of 50 ms. The phase change calculated from the I/Q components in that cycle was used to retrieve the vibration response This algorithm also has the lowest computational cost among the four algorithms. Thus, it is recommended in $\varphi$-OTDR systems with high dynamic performance.
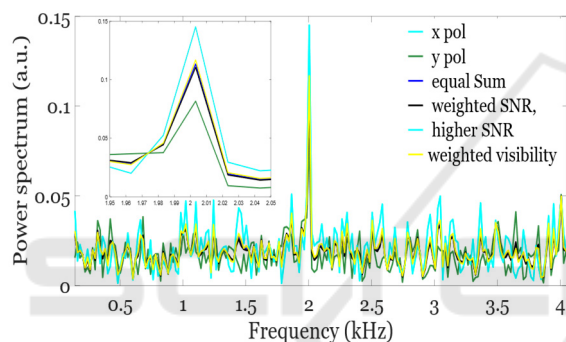


Figure 10: The responses of the four algorithms at the vibration of 2 kHz with respect to those of x and y polarizations.

## 5 CONCLUSIONS

In summary, we have proposed and experimentally demonstrated polarization fading mitigation in DAS based on homodyne detection in an unbalanced interferometer using delayed self-mixing of the Rayleigh backscattering traces. The technique has been used to measure small vibrations at the end of a 10-km fiber with vibration frequencies of 2 kHz. We have compared the use of four strategies to combine the demodulated phase obtained from the I/Q components of the fast and slow polarization axes. Experimental results show that, while phase combining strategies involving equal summation of the phase response and their weighing using interference visibility help to mitigate polarization fading, the selection of the phase computed from the polarization component with higher SNR in the in-phase component yields better results

as well as being the one requiring fewer computations. This approach is also more suitable for real-time measurements compared to those based on weighing the phase contributions or relative SNR of the in-phase component and the relative visibility of the amplitude of backscattering traces in both axes.

## REFERENCES

*90° Optical Hybrid*. Website: https://www.ixblue.com/photonics-space/90-optical hybrid/.

Bielecki, Z., Achtenberg, K., Kopytko, M. E., Mikołajczyk, J. A., Wojtas, J., & Rogalski, A. W. (2022). Review of photodetectors characterization methods. *Bulletin of the Polish Academy of Sciences, Technical Sciences*, *70*(2).

Cammarata, S., Velha, P., Palla, F., Di Pasquale, F., Saponara, S., & Faralli, S. (2022). 30 Gb/s NRZ Transmission with Lumped-Element Silicon Photonic Mach-Zehnder Modulator. *2022 IEEE Photonics Conference (IPC)*, 1–2.

Demise, A., Di Pasquale, F., & Muanenda, Y. (2023). A compact source for a distributed acoustic sensor using a miniaturized EYDFA and a direct digital synthesis module. *SPIE Future Sensing Technologies 2023*, *12327*, 368–374.

Demise, A., Di Pasquale, F., & Muanenda, Y. (2024). A Compact DAS Based on a Low Phase Noise DDS and Mini-EYDFA for Real-Time Vibration Measurements. *2024 IEEE Sensors Applications Symposium (SAS)*, 1–6.

Jin, Z., Chen, J., Chang, Y., Liu, Q., & He, Z. (2024). Silicon photonic integrated interrogator for fiber-optic distributed acoustic sensing. *Photonics Research*, *12*(3), 465–473.

Li, Y., Wang, Y., Xiao, L., Bai, Q., Liu, X., Gao, Y., Zhang, H., & Jin, B. (2022). Phase Demodulation Methods for Optical Fiber Vibration Sensing System: A Review. *IEEE Sensors Journal*, *22*(3), 1842–1866. IEEE Sensors Journal.

Liu, S., Yu, F., Hong, R., Xu, W., Shao, L., & Wang, F. (2022). Advances in phase-sensitive optical time-domain reflectometry. *Opto-Electronic Advances*, *5*(3), 200078–1.

Muanenda, Y. (2018). Recent Advances in Distributed Acoustic Sensing Based on Phase-Sensitive Optical Time Domain Reflectometry. *Journal of Sensors*, *2018*(1), 3897873.

Nur, A., & Muanenda, Y. (2024). Design and Evaluation of Real-Time Data Storage and Signal Processing in a Long-Range Distributed Acoustic Sensing (DAS) Using Cloud-Based Services. *Sensors*, *24*(18), Article 18.

Rao, Y., Wang, Z., Wu, H., Ran, Z., & Han, B. (2021). Recent Advances in Phase-Sensitive Optical Time Domain Reflectometry (Φ-OTDR). *Photonic Sensors*, *11*(1), 1–30.

Shaheen, S., Hicke, K., & Krebber, K. (2023). Phase-sensitive optical time domain reflectometry based on geometric phase measurement. *Scientific Reports*, *13*(1), 2862.

Stowe, D. W., Moore, D. R., & Priest, R. G. (1982). Polarization Fading in Fiber Interferometric Sensors. *IEEE Transactions on Microwave Theory and Techniques*, *30*(10), 1632–1635. IEEE Transactions on Microwave Theory and Techniques.

Uyar, F., Onat, T., Unal, C., Kartaloglu, T., Ozbay, E., & Ozdur, I. (2019). A direct detection fiber optic distributed acoustic sensor with a mean SNR of 7.3 dB at 102.7 km. *IEEE Photonics Journal*, *11*(6), 1–8.

Wang, Z., Zhang, L., Wang, S., Xue, N., Peng, F., Fan, M., Sun, W., Qian, X., Rao, J., & Rao, Y. (2016). Coherent Φ-OTDR based on I/Q demodulation and homodyne detection. *Optics Express*, *24*(2), 853–858.

Yang, G., Fan, X., Wang, S., Wang, B., Liu, Q., & He, Z. (2016). Long-range distributed vibration sensing based on phase extraction from phase-sensitive OTDR. *IEEE Photonics Journal*, *8*(3), 1–12.

Zhang, M., Wang, S., Zheng, Y., Yang, Y., Sa, X., & Zhang, L. (2016). Enhancement for Φ-OTDR performance by using narrow linewidth light source and signal processing. *Photonic Sensors*, *6*(1), 58–62.